Journal of Magnetic Resonance **138,** 220–224 (1999)
Article ID jmre.1999.1731, available online at http://www.idealibrary.com on IDEAL®

Magic Echo Solid-State NMR Imaging without a Rapidly Switchable Field Gradient

S. Matsui,[1] M. Nonaka, T. Nakai, and T. Inouye

Institute of Applied Physics, University of Tsukuba, Tsukuba, Ibaraki 305-8573, Japan

Received August 26, 1998; revised February 3, 1999

To relax the high-speed requirement imposed on the gradient system used in solid-state proton imaging, we propose two simple modifications of the magic echo imaging sequence, TREV-16TS. In the first modification, the applied gradient is inverted in the middle of the RF irradiation; the second modification utilizes a sinusoidal gradient synchronized with the RF sequence. It is estimated by experiments that as long as the RF amplitude is at least about 10 times stronger than the resonance offset induced by the gradient, the spatial resolution is not degraded significantly by the line narrowing deterioration due to the gradient applied during the on-resonance RF irradiation. The modifications allow commercially available standard gradients to be used for the magic echo imaging of solids.

Key Words: **magic echo; solid-state; NMR imaging; sinusoidal gradient.**

INTRODUCTION

Solid-state NMR imaging generally requires high-performance hardware (*1, 2*). In particular, for the imaging methods employing line narrowing techniques, the requirements imposed on the field gradient system are so stringent that they can hamper the methods' widespread use. In the multiple pulse imaging experiments (*3*), for instance, the gradient must be switched in less than 1 μs. This is because the multiple pulse line narrowing is based on the solid echo, and therefore the length of the RF-free windows for pulsed application of the gradient must be much shorter than the transverse relaxation time of the solid sample. This requirement can be relaxed to some extent by the use of multiple magic echoes for line narrowing (*4–7*), where the RF-free windows can be made as long as the transverse relaxation time (Fig. 1a). Nevertheless, standard gradient switching times commercially available are currently about the same as the transverse relaxation time, unless a specially designed gradient driver and/or specially wound gradient coils with a small inductance (a few microhenries) are used.

In this paper, to relax this requirement of fast gradient switching, we modify the gradient portion of the magic echo imaging sequence. We employ a standard gradient system that is commercially available for liquid-state imaging and can achieve a switching time of about 30 μs. In the modified sequences, the gradient is inverted during the RF irradiation, or alternatively a sinusoidal gradient is employed instead of the pulsed one. Experimental results indicate the conditions that must be satisfied to obtain high-resolution images with the gradient-modified magic echo sequences.

MODIFICATION OF THE GRADIENT SEQUENCE

When the gradient cannot be rapidly switched, we must resort to a continuous gradient combined with the original magic echo sequence, TREV-8 (*8*). The sequence TREV-8 refocuses the homonuclear (proton–proton) dipolar interaction only and scales down inhomogeneous interactions such as chemical shifts and heteronuclear dipolar interactions, exhibiting a relatively limited degree of line narrowing. Since the spatial resolution is proportional to the line-narrowing efficiency, better resolutions can be obtained by using the sequence TREV-16TS, modified for improved line narrowing (*4, 5*). Consequently, we have tried to devise imaging sequences using the TREV-16TS as shown in Fig. 1.

Figure 1a shows the ideal gradient pulse sequence we proposed previously (*4*). Here, the gradient pulses are applied only during the RF-free windows to avoid gradient interference with the RF line narrowing. The polarity of the gradient is inverted in synchrony with the RF pulse sequence. This is because spins are inverted successively by 180° pulses virtually inserted in the TREV-16TS sequence for additional refocusing of inhomogeneous interactions. The gradient switching must be rapid enough to ensure that gradient pulses can achieve maximal frequency encoding.

To attain the same frequency encoding by using a relatively slow gradient with a switching time of about 30 μs, which is equal to the time interval τ (Fig. 1), an initial conception is the use of the gradient sequence shown in Fig. 1b, where the gradient inversion is made at each center of the RF irradiation sandwiched by the 90° y pulses. This modification is useful when a gradient switching time is equal to or shorter than the time interval 2τ of the TREV-16TS sequence. Generally, as

[1] To whom correspondence should be addressed. E-mail: matsui@bk.tsukuba.ac.jp.

1090-7807/99 $30.00

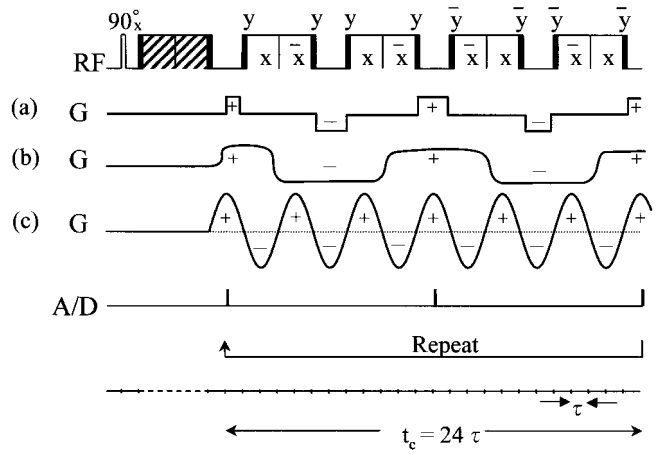

FIG. 1. Magic echo sequence, TREV-16TS, for solid-state imaging combined with ideally pulsed (a), nonideally pulsed (b), and sinusoidal (c) field gradients. On-resonance RF irradiations along x and $-x$ are sandwiched by 90° y pulses. This is called the magic sandwich. The hatched magic sandwich represents four magic sandwiches.

long as the RF field is strong compared to the gradient-induced resonance offset, the resonance offset can be neglected during the RF irradiation. The resonance offset is averaged out by the fast nutation about the RF field direction. Thus, the gradient sequence modified as Fig. 1b has the same effect as that of Fig. 1a. However, how much stronger the RF field should be to avoid possible interference between the gradient and the RF irradiation remains to be examined.

Another point to be noted in considering such interference is the gradient effect on the sandwiching 90° y pulses applied for the interconversion between the rotating (R) and tilted rotating (TR) frames (*8*). The gradient effect on the frame interconversion complicates the theoretical description of the interference effects, because the resultant spin flipping around the effective field deviates from the ideal 90° flipping about the y axis, not only in the flip angle but also in the flip axis direction. If the flip axis deviation can be ignored, the flip angle deviation remains, resulting in a spatial distribution of the tilted angle of the TR frame along the gradient direction. Although the tilted angle distribution matches the distribution of the nutation axis during the sandwiched RF irradiation under the presence of the gradient, the spatial distribution leads to incomplete refocusing of the homonuclear dipolar interaction. This is because for complete refocusing, the tilted angle must be uniformly 90° in space. The time intervals in the TREV-16TS sequence are set by assuming that the homonuclear dipolar interaction is scaled uniformly by the factor of $-\frac{1}{2}$ in the TR frame.

The use of the sinusoidal gradient waveform, shown in Fig. 1c, avoids this distribution effect on the frame interconversion, and is expected to provide a better resolution. The gradient-induced resonance offset will again be averaged out by the fast RF nutation. The sinusoidal time dependence of the gradient can be neglected, as long as its frequency is much lower than the RF nutation frequency.

For the RF nutation averaging of the gradient-induced resonance offset, the average Hamiltonian (AH) theory (*9*) tells us that because of the symmetry of the TREV-16TS sequence, all the odd-order AHs are zero in addition to the zeroth-order AH. Thus, the first nonzero term is the second-order AH. This suggests that the RF amplitude can be somewhat smaller than anticipated in both modifications.

An additional technical advantage in the use of sinusoidal gradient is that although the frequency components of the rectangular gradient pulses spread over a wide bandwidth including much higher frequency components than the frequency determined by the pulse width, the highest frequency component of the sinusoidal gradient waveform is simply the oscillation frequency. This significantly relaxes the high-speed requirement on the gradient system. The utility of the sinusoidal gradient for solid-state imaging was also described in other imaging schemes (*10*, *11*).

EXPERIMENTAL

Experiments were carried out on a homebuilt NMR imager and a Chemagnetics CMX300 Infinity, operating for protons at

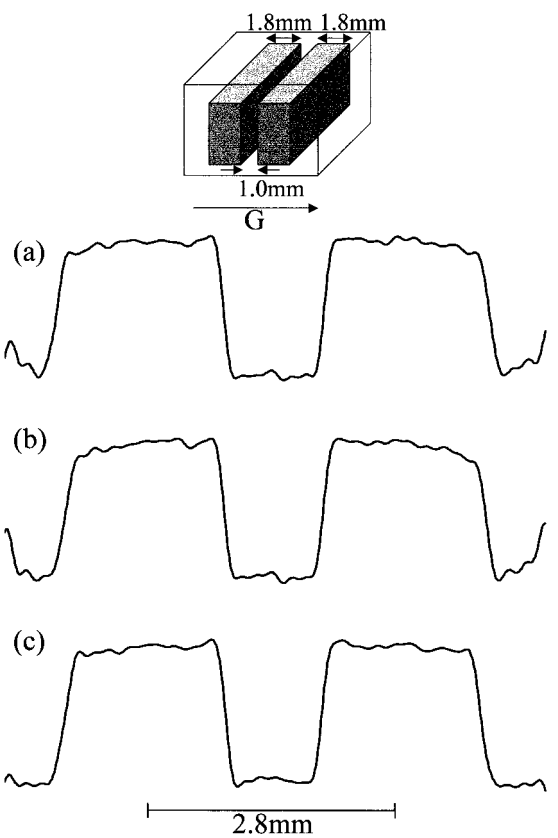

FIG. 2. Projections of the one-dimensional test sample obtained with the TREV-16TS sequence (τ = 30 μs) combined with the ideally pulsed (a), nonideally pulsed (b), and sinusoidal (c) gradients illustrated in Fig. 1. The RF amplitude was set at 100 kHz. A one-dimensional test sample of adamantane powder was measured on the homebuilt imager.

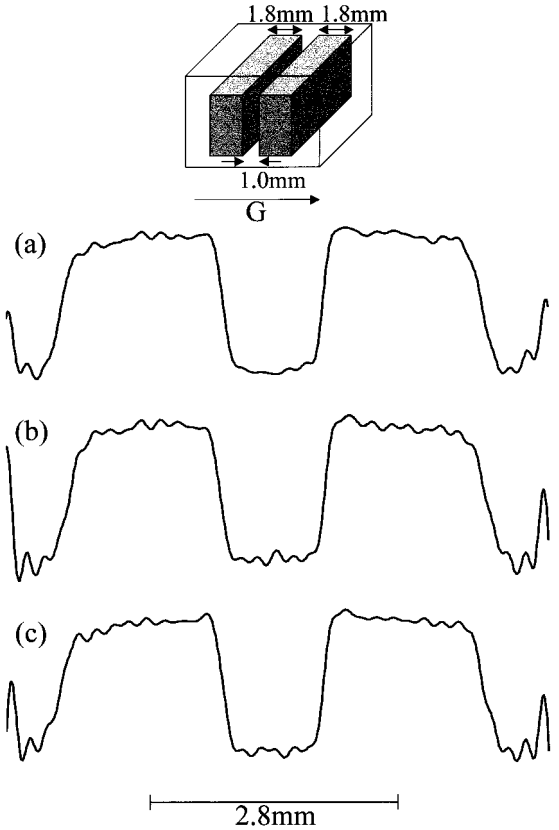

FIG. 3. Projections of the one-dimensional test sample obtained with the TREV-16TS sequence (τ = 30 μs) combined with the ideally pulsed (a), nonideally pulsed (b), and sinusoidal (c) field gradients illustrated in Fig. 1. The RF amplitude was set at 51 kHz. A one-dimensional test sample of adamantane powder was measured on the homebuilt imager.

60 and 300 MHz, respectively. The RF amplitude was variable between 100 and 21 kHz, depending on the experiment. The time interval τ of the magic echo pulse sequence (Fig. 1) was fixed at 30 μs. Suitably shaped adamantane powders, which exhibit a linewidth of about 14 kHz, were the test sample for all the experiments.

The gradient system in the homebuilt imager comprises a small coil with an inductance of a few microhenries and a high-speed driver with a bandwidth of about 1 MHz, achieving a high efficiency of 4.5 G/cm/A and a switching speed as fast as 3 μs. On the other hand, the inductance of the active-shielded gradient coils in the CMX300 was about 40 μH and the efficiency of the coils was ca. 1 G/cm/A. The bandwidth of the driver, Techron 7570, was 20 kHz. The sinusoidal waveforms were obtained by simply inserting a phase-linear Bessel low-pass filter (24dB/oct) prior to the final driver. By setting the filter cutoff frequency to the inversion rate, ¼τ (Fig. 1), successively inverting rectangular waveforms were converted to corresponding sinusoidal waves.

RESULTS AND DISCUSSION

Experiments with a Rapid Gradient System

To examine the gradient interference effects on the TREV-16TS line narrowing efficiency, it is necessary to vary the gradient amplitude relative to the RF amplitude. Since the imaging parameters are changed if the gradient is varied, we chose in the following experiments to vary the RF amplitude while keeping the gradient amplitude constant. Using the sequences shown in Figs. 1a, 1b, and 1c, we have measured projections of the one-dimensional test sample, which was aligned precisely to about $\pm 1°$ using a stepping motor. The results obtained by running the sequences on the homebuilt imager are shown in Figs. 2, 3, and 4.

Projections obtained at an RF amplitude of 100 kHz are shown in Fig. 2, where projections 2a, 2b, and 2c were measured by employing the ideally pulsed, nonideally pulsed, and sinusoidal gradients as shown in Figs. 1a, 1b, and 1c, respectively. It can be seen immediately that a high resolution of 100 μm or a better is achieved, and no significant difference is observed in resolution among the three projections. This is

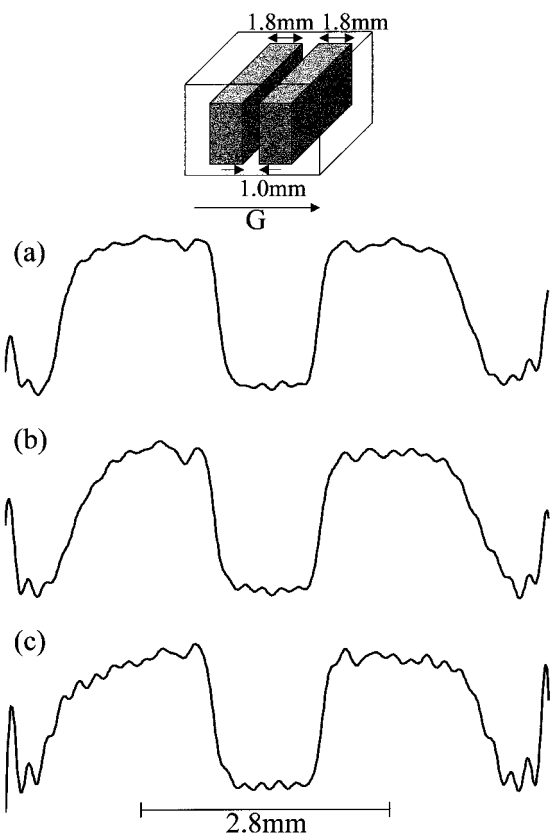

FIG. 4. Projections of the one-dimensional test sample obtained with the TREV-16TS sequence (τ = 30 μs) combined with the ideally pulsed (a), nonideally pulsed (b), and sinusoidal (c) field gradients illustrated in Fig. 1. The RF amplitude was set at 36 kHz. A one-dimensional test sample of adamantane powder was measured on the homebuilt imager.

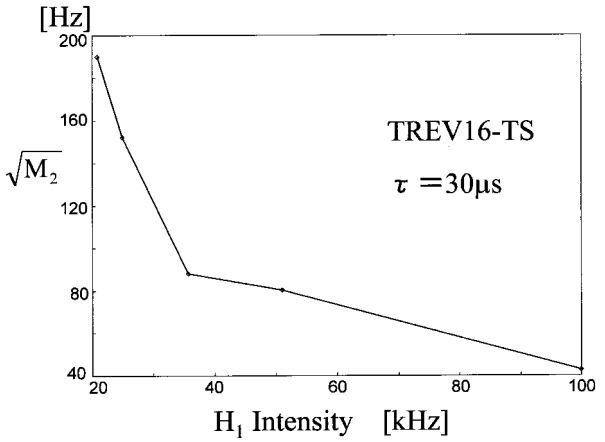

FIG. 5. TREV-16TS line narrowing efficiency plotted as a function of the RF amplitude. The square root of the second moment $\sqrt{M_2}$ of the narrowed proton line of the adamantane test sample was measured on the homebuilt imager. It can be seen that the line narrowing is quite effective when the RF field is stronger than about 36 kHz, whereas if it is weaker, it deteriorates rather rapidly.

reasonable because the RF amplitude of 100 kHz was much stronger than the maximum resonance offset ±4.2 kHz at both ends of the projections, as calculated by the applied gradient of about 4.4 G/cm. The RF nutation averaging of the gradient-induced resonance offset and the interconversion between the R and TR frames are almost perfect in this experimental condition.

Figure 3 shows projections measured in the same manner as in Fig. 2; the RF amplitude, however, was reduced to 51 kHz. Overall resolution is degraded by the somewhat reduced line narrowing efficiency resulting from the weaker RF amplitude. This can be confirmed by the experimental results shown in Fig. 5, where the line narrowing efficiency is plotted as a function of the RF amplitude. Only slight or essentially no difference is observable in resolution among the three projections in Fig. 3. However, the difference becomes much more pronounced in the similarly obtained projections shown in Fig. 4, where the RF amplitude was reduced even more to 36 kHz and the overall resolution becomes worse because of the decreased narrowing efficiency (Fig. 5). In particular, although the highest resolution is obtained in projection 4a, projection 4b exhibits the lowest resolution. Qualitatively, the difference between projections 4a and 4b can be ascribed to the two gradient interference effects mentioned above. On the other hand, the difference between projections 4b and 4c may be due to the gradient effect on the frame interconversion.

These experimental results indicate that to avoid resolution loss due to gradient effects, the RF amplitude should be at least about 10 times stronger than the gradient-induced resonance offset; the second modification, of using the sinusoidal gradient, is more tolerant of such resolution loss, as expected.

Experiments with a Slow Gradient System

To confirm the utility of the gradient-modified TREV-16TS sequences (Figs. 1b and 1c), experiments were conducted on the CMX300 Infinity, to which a standard gradient system designed for liquid-state imaging by JEOL was attached. The RF amplitude was about 68 kHz and the other imaging conditions were the same as those set on the homebuilt imager.

Figure 6 shows the experimental results, demonstrating the utility of the modified sequences. Projection 6a, which is displayed for comparison, was obtained with the TREV-8 sequence combined with an unswitched gradient. Projections 6b and 6c were measured by the gradient-modified TREV-16TS sequences as before. Of course, the ideal sequence in Fig. 1a was unusable here. Note the considerable improvement in resolution brought about by the use of the gradient-modified TREV-16TS sequences instead of the TREV-8 sequence. This improvement results from the different line narrowing efficiencies of the TREV-8 and TREV-16TS sequences, where the narrowing efficiencies were represented by $\sqrt{M_2}$ = 220 and

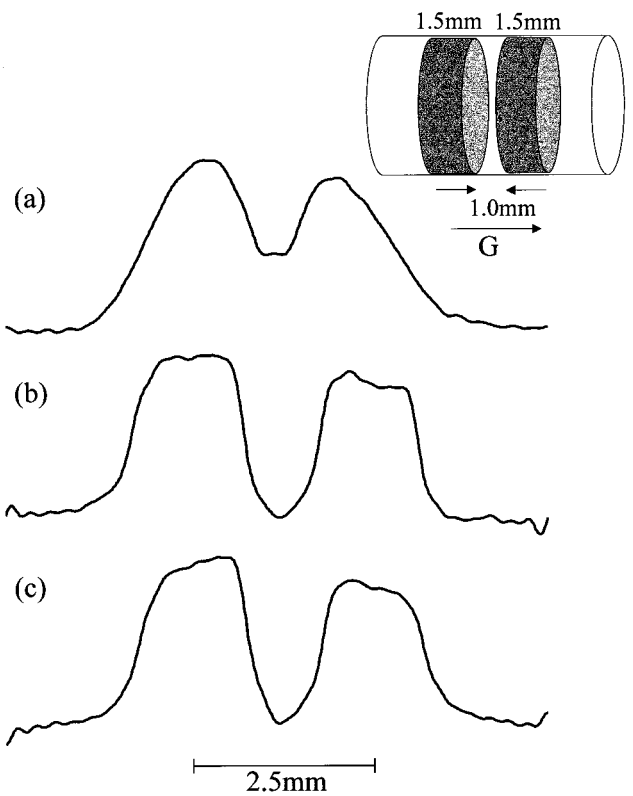

FIG. 6. Projections of the one-dimensional test sample of adamantane. Projection (a) was obtained with the TREV-8 sequence (τ = 30 μs) combined with an unswitched gradient. The TREV-16TS sequence (τ = 30 μs), combined with nonideally pulsed (Fig. 1b) and sinusoidal (Fig. 1c) field gradients, was used for the measurements of projections (b) and (c), respectively. The CMX300 imager was used for the measurements, and the RF amplitude was set at 68 kHz.

120 Hz, respectively. The degraded line narrowing compared to that obtained with the homebuilt imager ($\sqrt{M_2}$ = 50–60 Hz, Fig. 5) is due to the relatively poor RF homogeneity in the CMX300 Infinity. Essentially no difference can be observed between projections 6b and 6c, as in Fig. 3.

CONCLUSION

We have proposed two gradient-modified TREV-16TS imaging sequences for relaxing the high-speed requirement on the gradient system. Experiments made on the homebuilt imager and on the CMX300 Infinity have demonstrated the utility of the modifications. The use of the modified sequences permits the relatively slow gradient systems to be used, making the magic echo imaging of solids more easily accessible.

ACKNOWLEDGMENTS

The authors are grateful to Dr. Teruaki Fujito of JEOL for invaluable help in assembling the imaging probe for the CMX300 Infinity. This work was supported by the TARA (Tsukuba Advanced Research Alliance) of the University of Tsukuba and partly by Grant-in-Aid for Science Research 09650061 from the Ministry of Education, Science, and Culture of Japan.

REFERENCES

1. D. G. Cory, *Ann. Rep. NMR Spectrosc.* **24,** 87–180 (1992).
2. P. Blümler and B. Blümich, "NMR—Basic Principles and Progress," Vol. 30, pp. 209–277, Springer-Verlag, Berlin (1993).
3. D. G. Cory, J. B. Miller, and A. N. Garroway, *J. Magn. Reson.* **90,** 205–213 (1990).
4. S. Matsui, *Chem. Phys. Lett.* **179,** 187–190 (1991); S. Matsui, *J. Magn. Reson.* **95,** 149–153 (1991); S. Matsui, *J. Magn. Reson.* **98,** 618–621 (1992); S. Matsui, Y. Ogasawara, and T. Inouye, *J. Magn. Reson. A* **105,** 215–218 (1993); S. Matsui, M. Nonaka, T. Nakai, and T. Inouye, *Solid State NMR* **10,** 39–44 (1997).
5. S. Matsui, A. Uraoka, and T. Inouye, *J. Magn. Reson. A* **120,** 11–17 (1996).
6. F. Weigand, D. E. Demco, B. Blümich, and H. W. Spiess, *Solid State NMR* **6,** 357–365 (1996).
7. M. A. Hepp and J. B. Miller, *J. Magn. Reson. A* **111,** 62–69 (1994).
8. K. Takegoshi and C. A. McDowell, *Chem. Phys. Lett.* **116,** 100–104 (1985).
9. U. Haeberlen, "High Resolution NMR in Solids," Academic Press, New York (1976).
10. J. B. Miller and A. N. Garroway, *J. Magn. Reson.* **67,** 575–579 (1986).
11. S. L. Codd, M. J. D. Mallett, M. R. Halse, J. H. Strange, W. Vennart, and T. Van Doorn, *J. Magn. Reson. B* **113,** 214–221 (1996).